Acta Metallurgica Sinica (English Letters) (2022) 35:67–77
https://doi.org/10.1007/s40195-021-01333-y

In situ SR-CT Experimental Study on the Directional Sintering of High-Temperature Superconductor YBCO Materials in the Microwave Fields

Liangyuan Wang[1] · Lei Shen[2] · Yongcun Li[3] · Yuanjie Wang[1] · Yu Xiao[1] · Xingyi Zhang[2] · Feng Xu[1] · Xiaofang Hu[1]

Received: 29 June 2021 / Revised: 22 August 2021 / Accepted: 23 August 2021 / Published online: 3 November 2021

Abstract

$YBa_2Cu_3O_{7-x}$ (YBCO) is a kind of high-temperature superconducting material that has important application in information, energy, medical treatment, etc., and the superconducting properties of YBCO are closely related to its internal microstructure. In this study, the microwave heating method was adopted to prepare the YBCO materials. The internal 3D online evolution observation based on the synchrotron radiation computed tomography technology shows that there was directional grain growth phenomenon of YBCO during microwave sintering process. In local regions with special microstructure, these particles grew to the same point. Here, the theoretical models of single and multiple particles in the microwave electromagnetic fields were established. Based on these theoretical models and finite element analysis, it shows that the YBCO particles can modulate the distribution of electromagnetic fields, resulting in the significantly higher electric field intensity at the particle junctions than other regions. Moreover, there were very high electric field intensity and temperature gradients in the directions of particle growth. These factors were crucial in directional sintering. These results will provide theoretical basis and technical guidance for the controllable preparation and performance optimization of the internal microstructure of superconducting materials in the preparation process.

Keywords Synchrotron radiation computed tomography · Microwave sintering · Microstructure · In situ

1 Introduction

$YBa_2Cu_3O_{7-x}$ (YBCO) is a kind of high-temperature superconducting material with zero resistance and complete diamagnetism in superconducting state, which is widely used in information, energy, medical treatment, transportation and other fields [1–3]. Solid-phase sintering is widely used in the preparation of YBCO, which takes $BaCO_3$, Y_2O_3 and CuO powder as raw materials, through several processes such as mixing, calcination, grinding and sintering [4, 5]. The traditional sintering method is simple to operate, but the long time and high temperature of sintering process easily result in polycrystalline structure with large-angle grain boundaries [6]. The morphology, phase composition and grain orientation of YBCO have important effects on its superconducting properties [7–9]. Therefore, a new fabrication method to save energy, shorten time consumption and improve the superconducting performance of YBCO should be proposed.

Compared with traditional sintering, microwave sintering technology can reduce the sintering time and temperature,

Available online at http://link.springer.com/journal/40195.

✉ Xingyi Zhang
zhangxingyi@lzu.edu.cn

✉ Feng Xu
xufeng3@ustc.edu.cn

[1] CAS Key Laboratory of Mechanical Behavior and Design of Materials, Department of Modern Mechanics, CAS Center for Excellence in Complex System Mechanics, University of Science and Technology of China, Anhui 230027, China

[2] Key Laboratory of Mechanics on Disaster and Environment in Western China Attached to the Ministry of Education of China, Lanzhou University, Lanzhou 730000, China

[3] Shanxi Key Lab of Material Strength & Structural Impact, College of Mechanical and Vehicle Engineering, Taiyuan University of Technology, Taiyuan 030024, China

save energy and improve material properties [10, 11]. Microwave sintering is a method of densification by using the coupling of the special wave band of microwave and the basic fine structure of the material to generate heat, and the dielectric loss of the material in the electromagnetic field to heat the whole material to the sintering temperature [12, 13]. The microwave electromagnetic field makes the activation energy of sintering decrease and the diffusion coefficient of the material increase. Orlik et al. [14] confirmed that the microwave can reduce the preparation time from 12.5 to 1.5 h by using microwave sintering of barium titanate doped with calcium and zirconium. Compared with the traditional sintering of submicronic aluminum, the preparation time of microwave sintering is reduced from 180 to 60 min, and the grain size is reduced from 3.6 to 2.4 μm [15]. During microwave sintering, the material converts electromagnetic energy into heat energy. The thermal effect is different due to the difference of dielectric loss, morphology and arrangement of particles. This can be used to achieve selective sintering in space and prepare materials with improved microstructure and excellent properties [16–18], which indicates that the microwave heating may be a good YBCO preparation technology, but few studies are carried out in this area. So, the interaction mechanism between microwave and YBCO materials, and the properties as well as the microwave sintering mechanisms of YBCO material are still unclear.

Researchers usually observe the microstructure of YBCO after sintering by scanning electron microscopy (SEM), focusing on grain orientation, cracks and pores. The resolution of SEM image reaches nanometer level, but only a two-dimensional cut of the finished product can be obtained. As a new type of light source, synchrotron radiation has many outstanding advantages, such as high luminance, high photon flux and high collimation. Synchrotron radiation computed tomography technology (SR-CT) can realize real-time, three-dimensional and nondestructive observation of the internal microstructure of materials under the action of complex external field [19, 20]. The microstructure evolution of materials during microwave sintering can be observed and analyzed in the in situ way [21, 22]. In the experiment, some special and important evolution phenomena such as the local regions of directional sintering of the YBCO particles were observed. Through further analysis, it was speculated that the growth orientation of particles was closely related to the gradient distribution of microwave electromagnetic field. It helps us to deeply understand the interaction mechanism between microwave electromagnetic field and YBCO and realize the rapid preparation of YBCO by microwave sintering. Moreover, this was of great significance for regulating the microstructure and grain orientation of YBCO and improving the superconducting properties of the material.

2 Experimental Methods and Results

2.1 Experimental Apparatus and Methods

This experiment was carried out at the Shanghai synchrotron radiation source BL13W1 beam line station. The sintered sample was the high-temperature superconductor YBCO powders with the particle size of 20–80 μm. The internal microstructure evolution of YBCO powders during microwave sintering was observed online. The effective energy range of X-rays was 8 to 72 keV, and the X-ray energy was selected as 38 keV according to the absorption coefficient of YBCO. As shown in Fig. 1, the sample and rotating table were placed in a special microwave sintering furnace [23]. The sample was put into a quartz tube with a diameter of 2.5 mm and a height of 30 mm, and they were placed vertically on the microwave sintering cavity [24].

As shown in Fig. 2a, the transmission system avoided the damage of the high-temperature microwave environment to

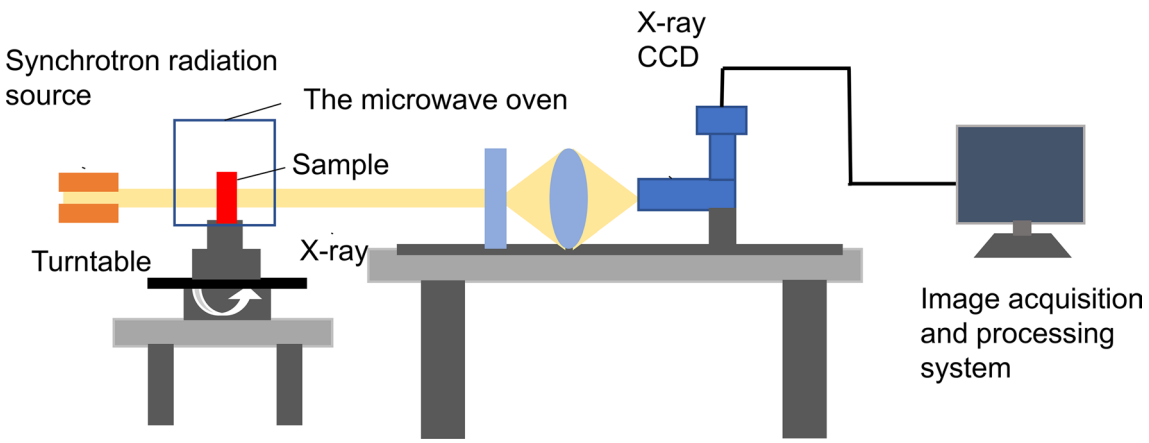

Fig. 1 SR-CT experimental device diagram of microwave sintering

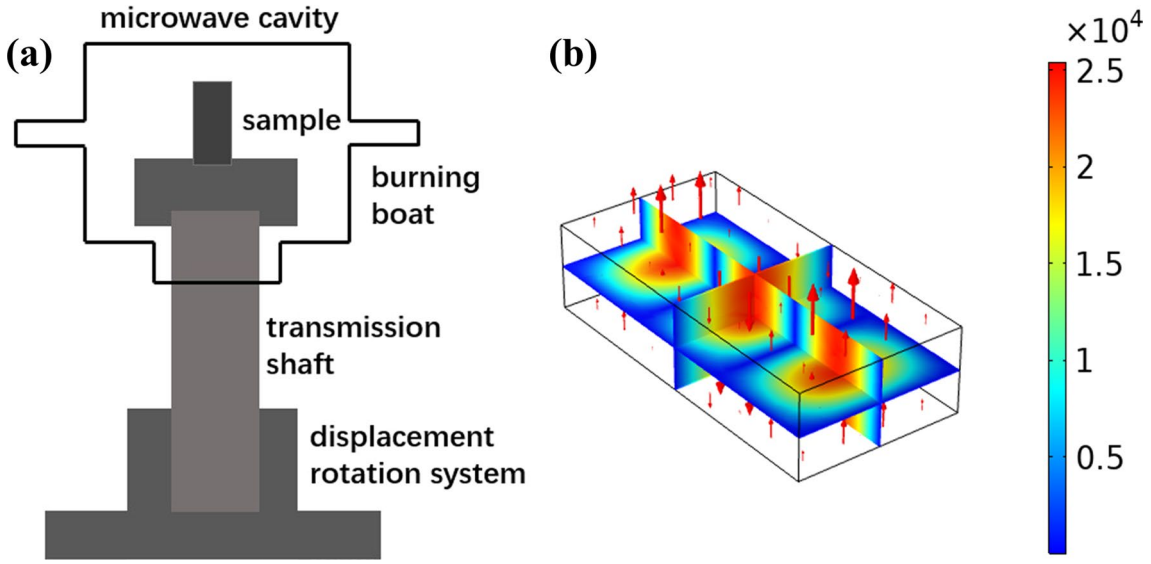

Fig. 2 **a** Schematic diagram of transmission system, **b** model of microwave resonator

the rotation displacement system during the experiment [25, 26]. The sample was placed on a high-temperature ceramic burning boat. The transmission shaft was inserted into the bottom of the burning boat, and the bottom of the transmission shaft passed through the coupling. The shaft device was connected with the displacement rotation system. In the microwave sintering device, the microwave source used a microwave generator with a frequency of 2.45 GHz and an output power of 0 to 3 kW. A small hole was set on the back side of the microwave oven, and an infrared thermometer was placed near this small hole. The measurement area of this infrared thermometer covered the upper surface of the sample [27]. The temperature measurement range was 500–2000 °C, and the error was ± 1.4 °C.

Figure 2b shows the single-mode resonant cavity model in the microwave sintering experiment. The cavity had a light hole at the same position of the cavity on the front and back. During the sintering process, the sample rotated at a high speed with the rotating table [28]. The synchrotron radiation X-ray passed through the sample through the light hole, and the CCD camera captured the projected image on the other side of the light hole [29]. The projected images of the sample were collected in the range of 180° at different times, and the projection interval was 1°. The CCD pixels were 2048 × 2048, the resolution was 0.33 μm, and the grayscale resolution was 16 bits.

The experiment was carried out in an air atmosphere, and the sintering temperature was controlled by adjusting the microwave power. The YBCO sample was heated from 25 to 1050 °C. After 1 h and 14 min, the microwave was turned off, and then the YBCO sample was naturally cooled to 25 °C.

2.2 Microstructure Evolution of YBCO

In order to study the difference of YBCO microstructure evolution, the reconstruction algorithm was adopted to reconstruct the three-dimensional microscopic morphology of the sample at different sintering time [30, 31]. The projected image of the YBCO sample was reconstructed by the filtered back-projection algorithm to obtain the tomogram of the sample. As shown in Fig. 3, the tomograms were assembled into a three-dimensional image using digital image processing technology.

As shown in Fig. 4, the cross sections of the sample were obtained at different time. The white area in the gray image represented the powder YBCO particles in the sintered body. The higher the gray level of the image, the higher the density of the position. Bright areas with higher grayscale represent particles, and dark areas with lower grayscale represent pores.

In Fig. 4, the two evolutionary regions were marked in rectangular boxes. Figures 5 and 6 show enlarged images of locally evolving regions 1 and 2. As it could be seen from the evolution diagram of YBCO at different time, the special evolution phenomenon of "tip connection" had occurred in local regions, and multiple particles were connected at "edges and corners" or "endpoints."

Figure 5a shows the image of region 1 before sintering. There was no sintering neck between particles 1, 2 and 3. Figure 5b shows the image of YBCO heated to the maximum temperature of 1050 °C. The edges and corners of particles 1, 2 and 3 were attached to the "tip," and the "tip" was marked with a blue box. Figure 5c shows the image of

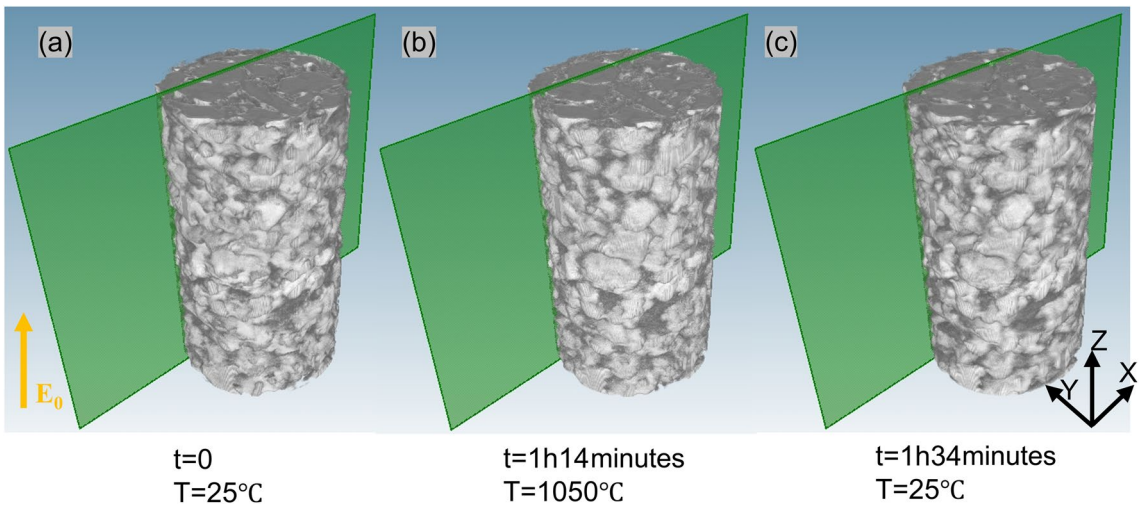

Fig. 3 Three-dimensional evolution diagram of YBCO: **a** initial state, **b** maximum temperature state, **c** final state

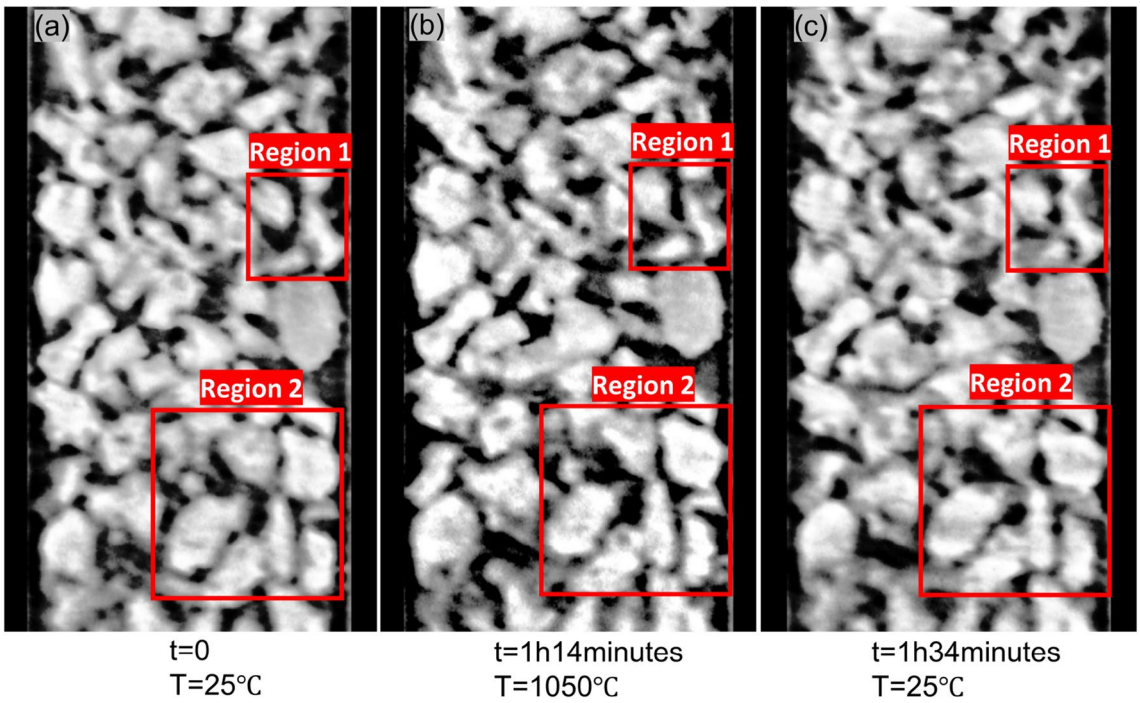

Fig. 4 Sectional evolution diagram of YBCO: **a** initial state, **b** maximum temperature state, **c** final state

YBCO cooled to temperature of 25 °C. Particles 1, 2 and 3 were still attached to the "tip."

Figure 6a shows the image of region 2 before sintering. There was no sintering neck between particles 1 and 4. Figure 6b shows the image of YBCO that heated to the maximum temperature of 1050 °C. The particles of 1 and 4 were attached to the "tip" 1. The particles of 5 and 6 were attached to the "tip" 2. The "tip" 1 and "tip" 2 were marked with a blue box and a yellow box. Figure 6c shows the image of YBCO cooled to temperature of 25 °C. Particles 3 and 5 were connected to "tip 1," while particles 5 and 6 were still connected to "tip 2."

Local evolution occurred in the sample, indicating that the temperature distribution was not uniform [25]. In the microwave sintering, the electromagnetic energy can be converted into heat energy, and the distribution of temperature field depends on the distribution of electromagnetic fields. In order to study the mechanism of directional sintering in

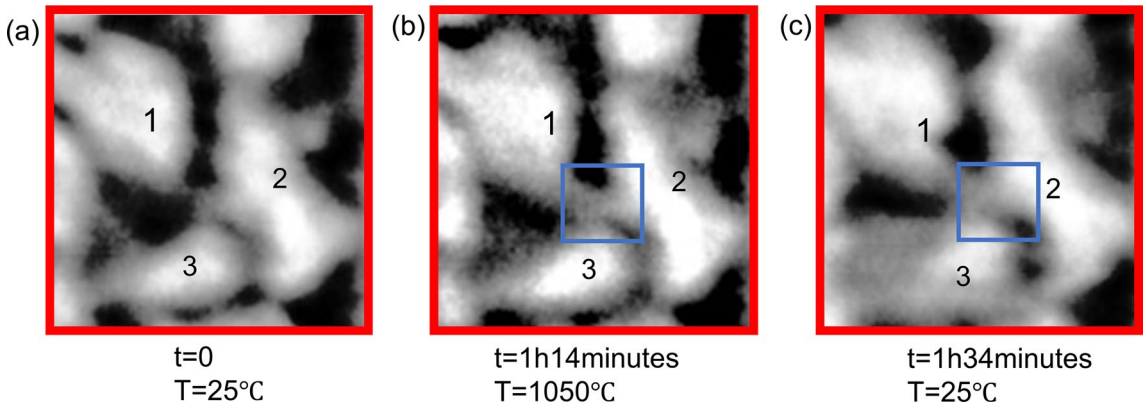

Fig. 5 Evolution diagram of region 1: **a** initial state, **b** maximum temperature state, **c** final state

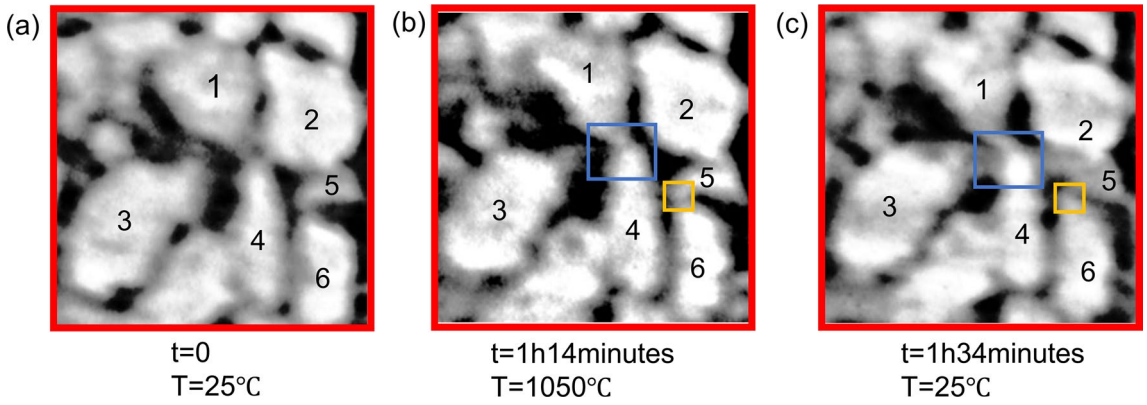

Fig. 6 Evolution diagram of region 2: **a** initial state, **b** maximum temperature state, **c** final state

YBCO, it is necessary to analyze the electric field distribution of particles.

3 Discussion

3.1 Temperature Gradient-Induced YBCO Directional Sintering

In order to further explain the experimental phenomenon, the specific distribution of particles in the local evolution region 1 and 2 were analyzed. As shown in Fig. 5, particles 2 and 3 formed a V-shaped structure. As shown in Fig. 6, particles 2 and 4 formed a V-shaped structure. The tip of the V-shaped structure was the final connection point of particles. The characteristics of this microstructure suggested that the V-shaped structure may be a key factor in the initiation of the "tip connection." The special microstructure led to the special distribution of electric field intensity in the sample. The special evolution of local regions may be related to the special distribution of electromagnetic fields on the particles.

Firstly, a theoretical model of an electrolyte particle in the electromagnetic field was established. As shown in Fig. 7a, the ellipsoid particle was constructed with a length of $2b$ and a diameter of $2a$. The center of the ellipsoid was set as the origin, and the rectangular coordinate system and spherical coordinate system were established.

The geometric equation of the ellipsoid is

$$\begin{cases} x = a\sin\theta\cos\varphi \\ y = a\sin\theta\sin\varphi \\ z = b\cos\theta \end{cases}, \quad (0 \le \theta \le \pi, 0 \le \varphi \le 2\pi, b > a). \quad (1)$$

Point C was located at the end of the long axis, Points D and C were both on the Z-axis, and the distance between them was d. The external electric field $\boldsymbol{E_0}$ was decomposed along the Y- and Z-axes as E_y and E_z.

On the basis of our previous study, the electric field intensity along the Z-axis at point D [32] can be obtained as

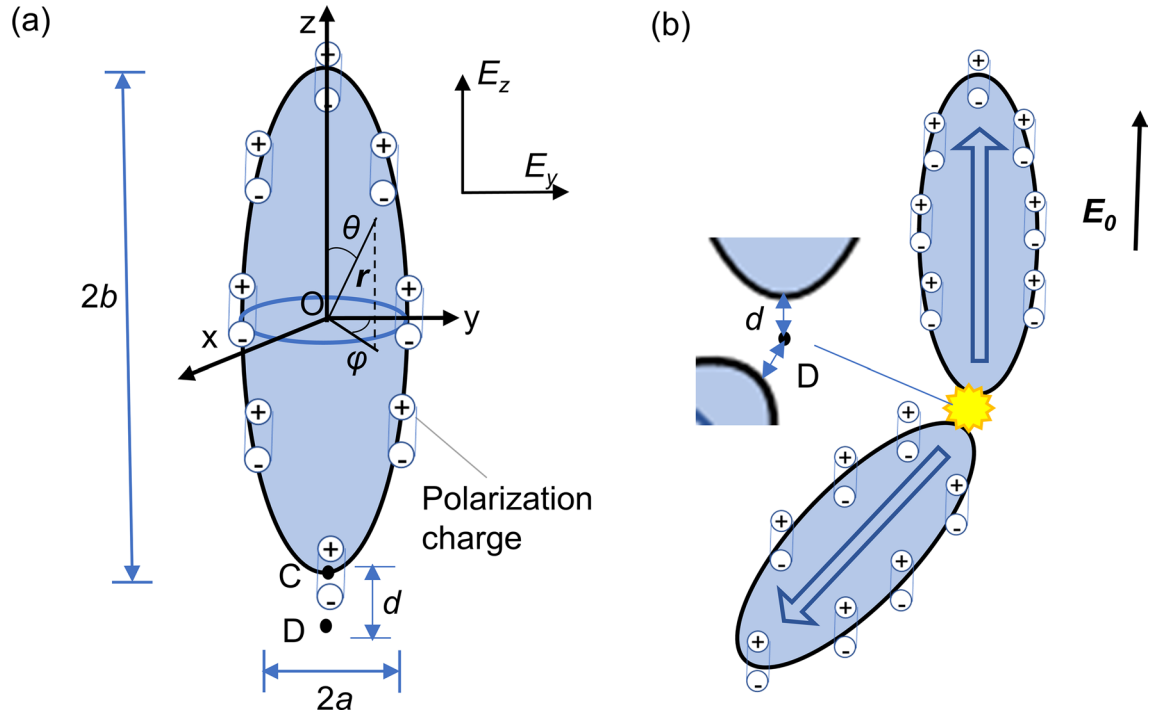

Fig. 7 **a** Geometric model of the ellipsoid particle, **b** V-shaped structural model

$$E_{Dz} = \frac{abE_z}{2C}\int \frac{\sin\theta\cos\theta(b\cos\theta + b + d)}{\left[a^2\sin^2\theta + (b\cos\theta + b + d)^2\right]^{3/2}}\mathrm{d}\theta. \quad (2)$$

The electric field intensity along the *Y*-axis at point D was

$$E_{Dy} = \iint \frac{a^2E_y\sin^2\theta\sin\varphi(b\cos\theta + b + d)}{2\pi(1-C)\left[a^2\sin^2\theta + (b\cos\theta + b + d)^2\right]^{3/2}}\mathrm{d}\theta\mathrm{d}\varphi. \quad (3)$$

The geometric parameter C is defined as

$$C = \int_1^{-1} \frac{-a^2b\cos^2\theta}{2\left(a^2\sin^2\theta + b^2\cos^2\theta\right)^{3/2}}\mathrm{d}\cos\theta. \quad (4)$$

YBCO materials were generally regarded as conductors at high temperatures. According to the uniqueness principle of electric field, the charge distribution law of conductor particles and dielectric particles with the same shape was exactly the same. Therefore, the electrolyte ellipsoid model in Fig. 7a could be used to calculate the electric field intensity in YBCO samples.

As shown in Fig. 7b, a theoretical model of V-shaped structure in an external electric field $\boldsymbol{E_0}$ was established. Particle 1 was placed vertically, and the angle between particle 2 and particle 1 was 135°. Geometric parameters $b = 100$ μm, $a = 25$ μm and $d = 20$ μm are set in Eqs. (2–4), and the electric field intensity generated by ellipsoid 1 and ellipsoid 2 at point D was calculated. All of the electric field intensity components were synthesized at point D, and the total electric field intensity of point D was 40.6 E_0. The tip of the V-shaped structure had a strong electric field, which can convert electromagnetic waves into heat energy. The tip became local heat zone, producing an uneven temperature field. The growth direction of particles was closely related to the distribution of temperature field. However, due to the complexity shape of the real particle morphology, it is difficult to obtain the accurate expression of the field intensity distribution and the corresponding value.

In order to obtain more detailed information of electric field distribution, the distribution of electric field in regions 1 and 2 was simulated by the finite element method. First, a 1 mm × 1 mm × 1 mm cubic space was constructed, and the external electric field was set to the same condition as the experiment. The sample was located in the middle of the single-mode cavity in Fig. 2b, where the electric field intensity was 25,000 V/m and the direction of the electric field was vertical. The microwave frequency was set as 2.45 GHz in the experiment. In this study, the microwave electromagnetic field mentioned above was taken as the standard electromagnetic field for numerical simulation. Models of different local regions were put into this space, and the model materials were YBCO. The parameters ε, μ and σ represent the relative permeability, relative permittivity and conductivity, and they are equal to 1, 1 and 5×10^5 S/m for the YBCO, respectively. The ε, μ and σ of the other regions

were 1, 1 and 0, respectively. The actual particle shape was irregular, but this study mainly focused on the electric field intensity neared the "tip." The geometric model only needed to approximate the shape of the particle in the "tip" area.

Figure 8a–c shows the evolution process of region 1. Particles 2 and 3 formed a V-shaped structure, and particle 1 grew to the tip of the V-shaped structure. Figure 8d, e shows the distribution of electric field intensity in region 1. Points A, B and C were selected along the boundary of particle 2, and points D, E and F were selected along the boundary of particle 3. Points C and D were located at the tip of the V-shaped structure. Point G was selected at the growth front of particle 1. Figure 8f shows the electric field intensity distribution of selected points. The electric field intensities at points A, B, C, D, E, F and G were 3.4×10^4 V/m, 1.9×10^4 V/m, 3.4×10^5 V/m, 2.6×10^5 V/m, 3.9×10^4 V/m, 2.9×10^4 V/m and 9×10^4 V/m, respectively. The electric field intensity at points C and D was much higher than that at other points. The uneven electric field distribution formed the electric field gradient, which was defined as a positive temperature gradient direction from low field intensity to high field intensity. As shown in Fig. 8e, the field intensity gradients along GA, GB, GC, GD, GE and GF directions were −958 V/(μm·m), −1187.5 V/(μm·m), 2974 V/(μm·m), 2173 V/(μm·m), −618 V/(μm·m) and −660 V/(μm·m), respectively. High electric field intensity gradients were formed along GC and GD directions. Areas with high electric fields had a strong ability to convert electromagnetic energy into heat. Therefore, the temperature of points C and D was significantly higher than that of point G. The arrows in Fig. 8e point to the rising direction of electric fields, which are consistent with the rising direction of temperature. High positive temperature gradients were formed along the GC and GD directions.

The growth direction of YBCO was driven by the temperature field. In the microwave sintering experiment process, YBCO was heated from 25 to 1050 °C. The temperature of the local area exceeded the melting point (melting point of YBCO, 1015 °C), resulting in a local liquid phase [2]. The temperature gradient produced surface tension on the liquid surface [33]. The liquid phase of particle 1 moved from point G to points C and D under the action of surface tension and gravity. After the microwave source was turned off, temperature of YBCO was reduced from 1050 to 25 °C. The liquid phase solidified without obvious change in shape.

Figure 9a–c shows the evolution process of region 2. Particles 2 and 4 formed a V-shaped structure, and particles 1, 3 and 6 grew to the tip of the V-shaped structure. Particles

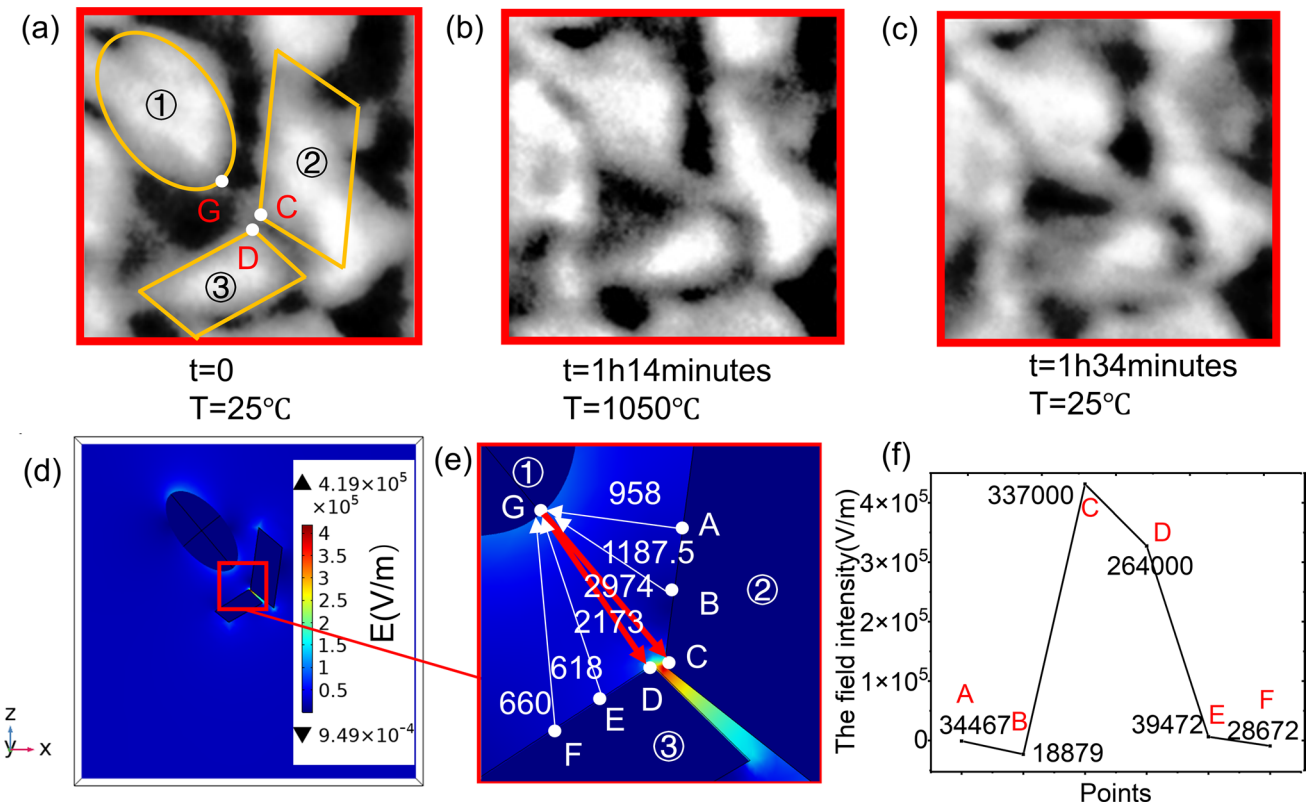

Fig. 8 **a** Initial state of region 1, **b** maximum temperature state of region 1, **c** final state of region 1; **d** electric field distribution of region 1, **e** electric field intensity gradient distribution, **f** electric field of points A, B, C, D, E and F

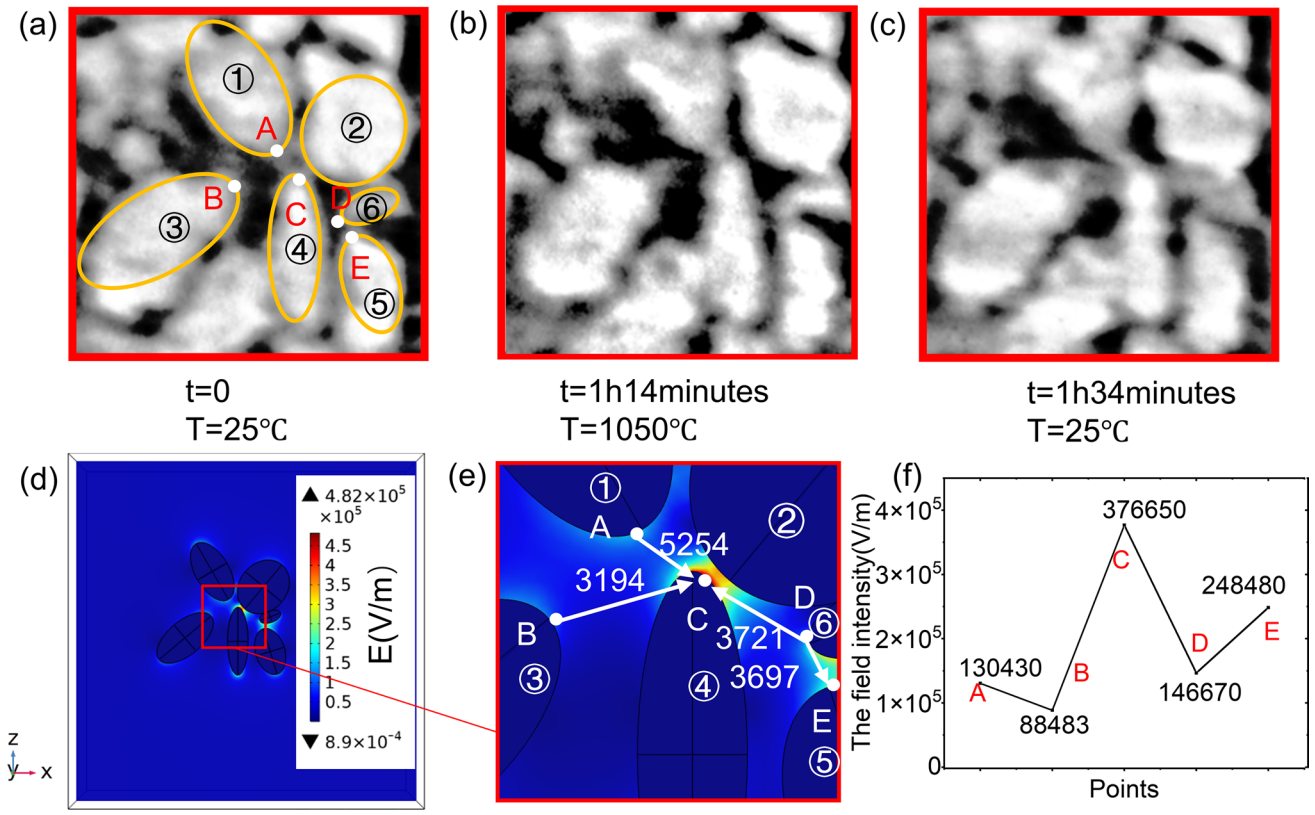

Fig. 9 **a** Initial state of region 2, **b** maximum temperature state of region 2, **c** final state of region 2, **d** electric field distribution of region 2, **e** electric field intensity gradient distribution, **f** electric field of points A, B, C, D and E

5 and 6 formed a V-shaped structure, and they connected together. Figure 9d, e shows the electricity field distribution of region 2. Points A, B, C, D and E were selected along the endpoints of particles 1, 3, 4, 6 and 5. Figure 9f shows the electric field intensity distribution of selected points. The electric field intensities at points A, B, C, D and E were 1.3×10^5 V/m, 8.8×10^4 V/m, 3.7×10^5 V/m, 1.5×10^5 V/m and 2.5×10^5 V/m. The electric field intensity at points C and E was much higher than that at other points. The field intensity gradients along AC, BC, DC and DE directions were 5254 V/(μm·m), 3194 V/(μm·m), 3712 V/(μm·m) and 3687 V/(μm·m). The temperature of points C and E was significantly higher than that of points A, B, D. The arrows in Fig. 9e point to the rising direction of electric fields, which are consistent with the rising direction of temperature. High positive temperature gradients were formed along the AC, BC, DC and DE directions. The growth direction of YBCO was driven by the temperature field [34, 35]. During the heating process, the liquid phase of particle 1 flowed from point A to point C. The liquid phase of particle 6 flowed from point D to point E. During the cooling process, the liquid phase solidified along the direction of the temperature gradient and particles grew from the solid–liquid interface to the tip of V-shaped structure. Particle 3 grew from point B to point C, and particle 6 grew from point D to point C.

The special V-shaped microstructure of the particles was the cause of directional sintering. The special V-shaped structure in the local region led to the special electric field distribution. A hot spot was generated in the local area, forming a positive temperature gradient from the periphery to the hot spot. The particles grew along the direction of the positive temperature gradient in the sintering process and finally connected to the hot spot.

3.2 Influence of YBCO Microstructure on Electric Field Distribution

In order to further understand the directional sintering phenomenon of YBCO, the relationship between the microstructure parameters of V-shaped structure and the temperature field driving mechanism was explored. In this section, the influence of orientation and arrangement of particles in the V-shaped structure on the electric field and temperature field was analyzed.

Firstly, the effect of the microstructure parameters of a single particle on the distribution of electric field intensity was simulated. The ellipsoid 1 model with 50 μm in axes

A and B and 200 μm in axis C was constructed. Axes A, B and C of the ellipsoid were parallel to axes *X*, *Y* and *Z*. Model 1 was placed into the standard electromagnetic field established in Fig. 8d. The ratio of electric field intensity *E* to external electric field intensity E_0 at a point was defined as electric field enhancement coefficient *f*, $f = E/E_0$. The particle orientation angle was defined as the included angle between the long axis and the *Z*-axis. Figure 10a–c shows the distribution of electric field intensity in particle 1 with different orientations. Figure 10d shows the electric field enhancement coefficient *fc* at the point C under different orientation angles θ. As θ increased, *fc* decreased gradually. When orientation angle θ was 0, the electric field enhancement effect at point C was the best.

Many particles in the actual sample were close together; it was necessary to simulate the distribution of electric field intensity of two particles in different arrangements. Figure 11a–c shows the distribution of electric field intensity of particles in different arrangement. Figure 11a shows the electric field intensity distribution of case 1. Two ellipsoidal particles with a length of 200 μm and a diameter of 50 μm were constructed. The long axis was kept in the same vertical line and parallel to the direction of the electric field. The distance between the two particles was 20 μm. When the orientation angle of the two particles was 0, the electric field intensity in the area between the two particles was significantly enhanced. Case 2 was constructed, and the particle orientation in case 1 was increased to 90°. Figure 11b shows the electric field intensity distribution of case 2. The field strength in the region between the two particle tips did not increase significantly. Case 3 was constructed. The long axis of the two particles was kept parallel to the *Z*-axis, while the short axis was kept on the same level and parallel to the *X*-axis. Figure 11c shows the electric field distribution of case 3, and the field intensity in the area near the two particles did not significantly increase. This indicated that the field strength at the tip of the V-shaped structure was enhanced mainly due to the effect of vertical particles. Moreover, when the angle between the two particles of the V-shaped structure was 180° and the long axis was parallel to the direction of the electric field, the electric field enhancement at the tip was best.

The proximity of particles had an important effect on electric field distribution. The particle model of Fig. 11a was constructed. Figure 11d shows the electric field enhancement coefficients of point D at the midpoint of the two particle

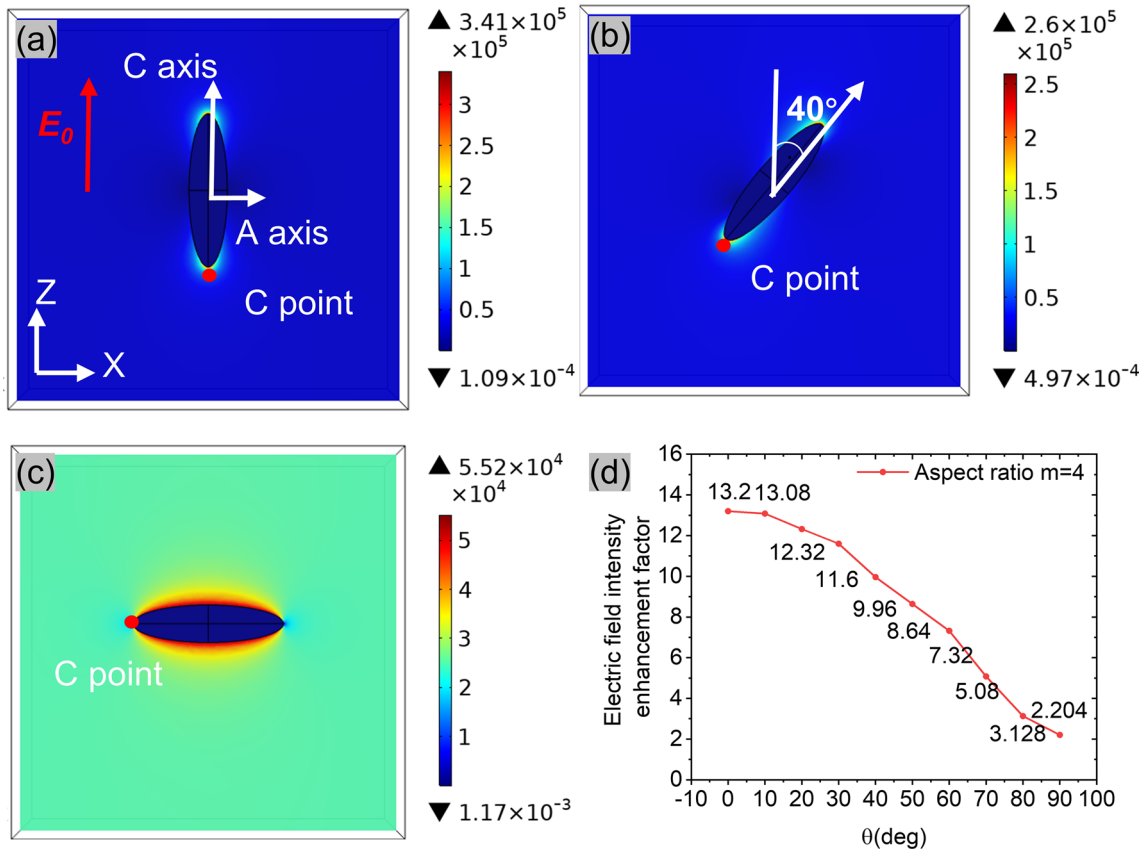

Fig. 10 **a–c** Electric field intensity distribution of different orientations: **a** $\theta = 0$, **b** $\theta = 40°$, **c** $\theta = 90°$, **d** electric field enhancement coefficient *fc* of different orientation angles θ

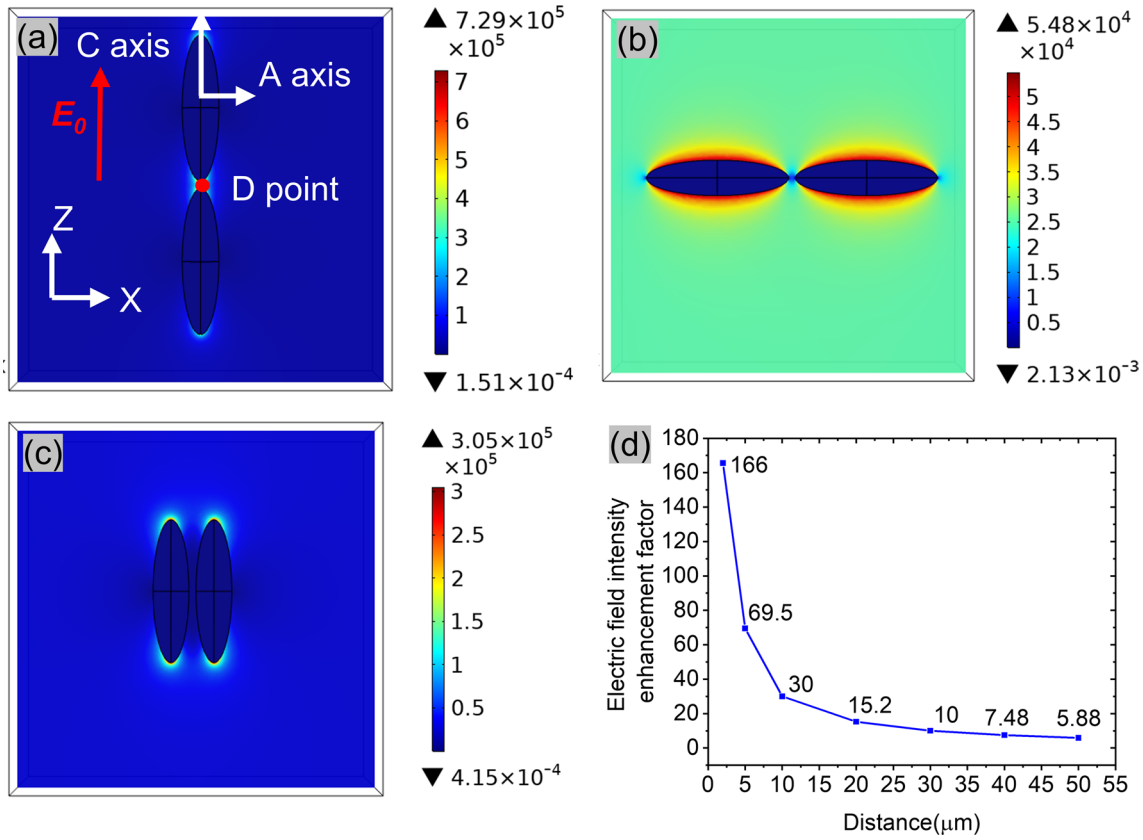

Fig. 11 **a–c** Electric field intensity distribution of different arrangements: **a** case 1, **b** case 2, **c** case 3, **d** electric field enhancement coefficient f_D of different distances in case 1

tips. When the distance was increased from 2 to 50 μm, the electric field enhancement coefficient decreased from 170 to 10. This indicated that the closer the two particles were in this arrangement, the better the tip enhancement effect was.

Through the above simulation, we had a further understanding of the relationship between the V-shaped structure and the temperature driving mechanism. When there are two particles in the electric field forming a V-shaped structure, keep the long axes of the two particles on the same line and parallel to the direction of the electric field. Set the distance between the two particles as small as possible without touching. A local hot zone could be formed at the tip of the V-shaped structure. Fabrication of such a V-shaped structure in the sample enables YBCO to undergo directional sintering. It is of great significance to fabricate YBCO with specific microstructures.

4 Conclusions

In this study, three-dimensional evolution of YBCO during microwave sintering was observed by SR-CT technology. It was found that some special local evolution occurred in YBCO, and the growth of YBCO particles was directional. All of these regions had a common V-shaped microstructure. The distribution of electric field intensity of single ellipsoid particle and V-shaped particle in electric field was deduced theoretically. It was found that the intensity of electric field at the tip of the V-shaped structure was greatly enhanced. The tip became a local thermal area and produced a temperature gradient from the tip to the periphery. Particles grew under the drive of temperature field. During the heating process, the liquid phase attached to the tip under the combined action of gravity and surface tension. In the cooling process, the particles grew along the direction of the temperature gradient, from the solid–liquid interface to the local hot zone. By simulating the electric field distribution under different microstructures, the temperature driving mechanism was further understood. Place the long axes of the two particles in a straight line parallel to the direction of the electric field. When two particles are close together, the electric field at the tip of the particle is greatly enhanced.

Acknowledgements This work was financially supported by the National Natural Science Foundation of China (No. U1832216, No.

11627901), the Major Program of the National Science Foundation of China (No. 11890683) and the National Key Research and Development Program of China (No. 2017YFA0403803)

Declarations

Conflict of interest The authors state that there are no conflicts of interest to disclose.

References

[1] N.M. Alford, J.D. Birchall, W.J. Clegg, M.A. Harmer, K. Kendall, D.H. Jones, J. Mater. Sci. **23**, 761 (1988)
[2] T. Nishio, Y. Itoh, F. Ogasawara, M. Suganuma, Y. Yamada, U. Mizutani, J. Mater. Sci. **24**, 3228 (1989)
[3] W.J. Carr, C. Oberly, IEEE Trans. Appl. Supercond. **9**, 1457 (1999)
[4] P. Diko, R. Pagáčová, K. Zmorayová, V. Kuchárová, L. Vojtkova, V. Antal, V. Kavecansky, J. Am. Ceram. Soc. **104**, 740 (2021)
[5] L. Pathak, S.K. Mishra, Supercond. Sci. Technol. **18**, 67 (2005)
[6] H. Dong, R. Hu, J.S. Li, H.C. Kou, X.Y. Xue, H. Chang, H.T. Cao, L. Zhou, Trans. Nonferrous Met. Soc. China **18**, 1139 (2008)
[7] R. Hu, H. Dong, J.S. Li, H.C. Kou, X.Y. Xue, H. Chang, H.T. Cao, L. Zhou, Rare Metal Mat. Eng. **37**, 854 (2008)
[8] D. Volochová, V. Kavečanský, V. Antal, P. Diko, X. Yao, Supercond. Sci. Technol. **29**, 044004 (2016)
[9] R. Teranishi, A. Mitani, K. Yamada, N. Mori, M. Mukaida, M. Miura, K. Nakaoka, T. Izumi, Y. Shiohara, Phys. C **469**, 1349 (2009)
[10] J. Zhang, X. Wei, X. Yang, W. Nie, Y. Ai, W. He, Mater. Sci. Eng. A **815**, 141273 (2021)
[11] Q. Li, Y. Ling, H. Zheng, G. Chen, J. Chen, S. Koppala, Q. Jiang, K. Li, M. Omran, L. Gao, Ceram. Int. **47**, 15849 (2021)
[12] H. Takahashi, Y. Numamoto, J. Tani, S. Tsurekawa, Jpn. J. Appl. Phys. **45**, 7405 (2006)
[13] H. Fukushima, T. Noritake, H. Hideo, J. Ceram. Soc. Jpn. **108**, 132 (2000)
[14] K. Orlik, Y. Lorgouilloux, P. Marchet, A. Thuault, F. Jean, M. Rguiti, C. Courtois, J. Eur. Ceram. Soc. **40**, 1212 (2020)
[15] M. Mizuno, S. Obata, S. Takayama, S. Ito, N. Kato, T. Hirai, M. Sato, J. Eur. Ceram. Soc. **24**, 387 (2004)
[16] K.H. Brosnan, G. Messing, D. Agrawal, J. Am. Ceram. Soc. **86**, 1307 (2003)
[17] M.I. Jones, M. Valecillos, K. Hirao, J. Ceram. Soc. Jpn. **109**, 761 (2001)
[18] K. Rybakov, S. Egorov, A. Eremeev, V. Kholoptsev, I. Plotnikov, A.A. Sorokin, J. Mater. Res. **34**, 2620 (2019)
[19] F. Xu, W. Liu, Y. Xiao, B. Dong, X. Hu, X. Wu, Appl. Phys. Lett. **110**, 101904 (2017)
[20] Z. Ding, N. Zhang, L. Yu, W. Lu, Q. Hu, Acta Metall. Sin. (Engl. Lett.) **34**, 145 (2021)
[21] F. Xu, X. Hu, B. Lu, J. Zhao, X. Wu, Q. Yuan, J. Inorg. Mater. **24**, 175 (2009)
[22] Y. Xiao, F. Xu, X.F. Hu, Y.C. Li, W.C. Liu, B. Dong, Metals **6**, 9 (2016)
[23] F. Xu, Y. Xiao, X. Hu, B. Dong, Y. Li, J. Instrum. **11**, C02074-C2081 (2016)
[24] W. Liu, F. Xu, Y. Li, X. Hu, B. Dong, X. Yu, Materials **9**, 120 (2016)
[25] F. Xu, W. Liu, X. Yu, B. Dong, X. Hu, X. Wu, Appl. Phys. Lett. **110**, 101904 (2017)
[26] B. Dong, X. Yu, F. Xu, X. Hu, W. Liu, J. Alloys Compd. **749**, 103 (2018)
[27] Y. Xiao, F. Xu, B. Dong, W.C. Liu, X.F. Hu, Metals **7**, 47 (2017)
[28] Y. Xiao, F. Xu, X.F. Hu, Y.C. Li, B. Dong, Metals **6**, 9 (2016)
[29] F. Xu, B. Dong, X. Hu, Y. Wang, W. Liu, Y. Li, Ceram. Int. **42**, 8296 (2016)
[30] L. Hou, Q. Zhang, J. Yang, X. Cai, Q. Chen, Nucl. Eng. Technol. **53**, 2348 (2021)
[31] W. Cho, J. Shin, K.T. Kim, Sci. Rep. (2021). https://doi.org/10.1038/s41598-021-92454-y
[32] Y. Li, F. Xu, X. Hu, D. Kang, T. Xiao, X. Wu, Acta Mater. **66**, 293 (2014)
[33] S.C. Hardy, J. Colloid Interface Sci. **69**, 157 (1979)
[34] L. Ma, R. Hu, J. Li, H. Kou, H. Fu, L. Zhou, Rare Metal Mat. Eng. **2**, 251 (2008)
[35] R. Hu, D. Hao, J. Li, H. Kou, X. Xue, H. Chang, H. Cao, L. Zhou, Rare Metal Mat. Eng. **37**, 857 (2008)